Fluid dynamic simulation of CrO2(OH)2 volatilization and gas phase evolution during the oxidation of a chromia forming alloy

Loïc Oger, Hugues Vergnes, Brigitte Caussat, Daniel Monceau, Aurélie Vande Put

Fluid Dynamic Simulation of $CrO_2(OH)_2$ volatilization and gas phase evolution during the oxidation of a chromia forming alloy

L. Oger[1,*], H. Vergnes[2], B. Caussat[2], D. Monceau[1] and A. Vande Put[1]

[1] CIRIMAT, Université de Toulouse, CNRS, INP-ENSIACET, 4 Allée Emile Monso, BP 44362, 31030 Toulouse Cedex 4, France

[2] LGC, Université de Toulouse, CNRS, INP-ENSIACET, 4 Allée Emile Monso, CS 84234, 31030 Toulouse Cedex 4, France

[*] Corresponding author. Tel.: +33 (0)5 34 32 34 16

*E-mail addres*s: loic.oger@toulouse-inp.fr ; l.loic.oger@gmail.com

Abstract: The influence of the chromia volatilization on the oxidation kinetics of Inconel 625 was investigated at 900 °C under flowing wet air (74%N_2-18.5%O_2-7.5%H_2O) through an interdisciplinary approach, coupling experiments and gas phase simulation. Oxidation tests showed a strong decrease in the volatilization rate of lined-up samples from the inlet to the outlet of a horizontal tubular furnace. Gas phase simulation allowed to relate it to an increase in the $CrO_2(OH)_2$ partial pressure along the tube. Considering gas composition changes appears as essential to provide correct interpretation of oxidation test results in humid and oxidizing environments.

Keywords: Nickel (A), Superalloys (A), Weight loss (B), Modeling studies (B), Oxidation (C).

1. Introduction

Chromia forming alloys, especially iron-base and nickel-base alloys, are in widespread use for applications at high temperature [1–5]. Their resistance against oxidation at high temperature depends on their ability to form a protective Cr_2O_3 scale. However, in many industrial applications, among which turbine blades [1,6], jet engines [7,8] or solid oxide fuel cells (SOFC) [1,9], the presence of water vapor in the oxidizing environment strongly

influences the oxide scale stability and kinetics of growth. Several studies attributed this phenomenon to the transformation of solid Cr_2O_3 into various volatile species identified as CrO_3 [10–14], $CrO_2(OH)$ [13] and $CrO_2(OH)_2$ [15] depending on the experimental conditions. More specifically, Opila *et al.* [16] showed by experimental and theoretical approaches that $CrO_2(OH)_2$ was the major species formed between 600 and 900 °C when Cr_2O_3 was exposed to water vapor and oxygen, according to *Reaction 1*. This was confirmed by other authors [2,7,17,18].

$$\frac{1}{2}Cr_2O_3(s) + \frac{3}{4}O_2(g) + H_2O(g) = CrO_2(OH)_2(g) \qquad \text{(Reaction 1)}$$

The main detrimental effect of Cr-volatilization reported in the literature is a breakaway on Fe-Cr alloys [3,19–23]. Asteman *et al.* [21,23] observed this phenomenon on a 304L alloy exposed to O_2+40vol%H_2O between 500 and 800 °C. They observed an enhanced Cr-depletion at the alloy/oxide interface leading to a decrease in the activity of Cr. As a consequence, the formation of a fast-growing non-protective Fe-oxide was then favoured, leading to a decrease in the oxidation resistance of the alloy. Concerning the Ni-base alloys containing low Fe-amounts, especially like the Inconel 625 (~1 at%), the formation of Fe-oxide scales is no expected [24] but several authors observed microstructural changes of the protective scale in humid air (up to 19 vol% H_2O) between 600 and 900 °C [17,18,25,26]. Indeed, the chromia scale was shown to be partially replaced by NiO or $NiCr_2O_4$ which are less protective and thus detrimental for the corrosion behavior of the alloys [25]. In experimental conditions close to industrial applications (flowing Air+6 vol% H_2O with a gas velocity of 6 m/s at 900 °C), Huczkowski *et al.* [25] observed the formation of a mixed oxide $CrNbO_4$ after 1000 h of oxidation. This was attributed to a decrease in the Cr concentration at the oxide/alloy interface beneath a critical level. This was also observed by Romedenne *et al.* [17] who studied the lifetime of a 625 alloy exposed in flowing air + 10% H_2O at 800°C: after 8000 h, the Cr_2O_3 layer was shown to be locally replaced by the rapid growth of less protective spinel oxide nodules.

Understanding the influence of water vapor on oxidation kinetics therefore appears to be an increasingly studied issue [27–31]. Most of the literature focuses on the changes in the oxidation kinetics and the oxide scale microstructure and morphology due to the presence of water in the oxidant environment, but few of the authors consider the evolution of the gas phase composition during the oxidation tests. Young and Pint [32] and Holcomb *et al*. [1] first evocated a possible change of the gaseous environment while the volatilization process occurs. Indeed, the volatile species partial pressure would increase just over the oxide scale, which would lead to a decrease in the volatilization kinetics as the reaction progresses. In particular, in their study, Holcomb *et al.* [1] calculated the Cr_2O_3 volatilization rate in a superheater considering that the water vapor-rich environment could be enriched in volatile species. This was considered in their calculation thanks to a methodology based on empirical correlations using dimensionless numbers. The saturation of the gaseous environment in $CrO_2(OH)_2$ was shown to lead to a decrease of 80% of the volatilization rate. In their recent work, Jacobson *et al.* [14] combined Computational Fluid Dynamics (CFD) simulations with experiments to describe the volatilization occurring at the surface of one single SiO_2 coupon exposed at 1650 °C. They demonstrated that in a gas mixture flowing through a tubular furnace, volatilized species were released at the coupon surface before being swept down through the furnace by the incoming flow. Considering one only coupon, the consequences are limited: the flow allows a continuous renewal of the environment around the sample and thus the volatilization kinetics is not modified. However, considering several lined-up samples as this is in usual cases, what would be the consequences of gas phase changes? It is reasonable to expect that the volatilization occurring at the first sample surface would modify the gas composition underwent by the following samples and thus would influence their oxidation behavior. The same phenomenon could be observed in industrial metallic pipes crossed by wet hot oxidant gases where heterogeneous behaviors could be observed along the pipes. However, this phenomenon which could lead to misinterpret the results is usually not taken into account in the majority of experimental studies.

In this framework, the present study investigates the influence of the chromia scale volatilization on the oxidation kinetics of a Ni-base alloy regarding the evolution of the gas phase composition. The specificity of this study lies in the coupling of experimental and CFD approaches to describe the evolution of the gaseous environment composition. As demonstrated on SiO_2 by Jacobson *et al.* [14], this interdisciplinary approach allows to deepen the understanding of the volatilization mechanism by simulating the surface volatilization reactions and the resulting evolution of the gas phase composition.

This paper reports high temperature oxidation tests which were carried out at 900 °C under a flowing wet air (74%N_2-18.5%O_2-7.5%H_2O) and quasi-static laboratory air. Inconel 625 was chosen for its ability to form, in the chosen experimental conditions, a dense Cr_2O_3 scale without spinel (e.g. $MnCr_2O_4$) that could decrease Cr activity at the outer surface of the oxide scale and thus reduce the volatilization rate [7,25,33]. This specific case was considered to allow a first analysis of the gas phase composition during the volatilization. This article focuses on the initial stages of oxidation and chromium loss due to volatilization, in other words, it is not concerned with the very long times that lead to a breakaway oxidation when the Cr content below the oxide layer becomes insufficient to ensure the formation of chromia. Three coupons were lined up in the horizontal furnace in order to analyze the influence of the gaseous composition on the oxidation kinetics at the surface of each of them. In this respect, flow rates of 200 sccm and 500 sccm were chosen (i.e. gas velocities of 6 $mm.s^{-1}$ and 1.4 $cm.s^{-1}$ respectively at 900 °C in the empty surface area of the furnace). These gas velocities are low as compared to main in-service conditions (velocities of 3 $m.s^{-1}$ and close to 7 $m.s^{-1}$ are generally reached by gas turbine exhaust steam [34] and SOFC gas channels [35] respectively), but they are typical of what is used in many laboratory studies. They were chosen to exacerbate the phenomenon of gas phase enrichment by the volatile species and its influence on the oxidation behavior of each sample. Higher velocities could have hidden this phenomenon. In addition, for the configuration using flowing wet air, the local gas velocity and temperature, the surface volatilization reaction on each coupon and the gas mixture evolution were studied by CFD

simulations in order to better understand the experimental results. The aim was to develop a model which did not require empirical relations to determine mass transfer coefficients and that could be a starting point for correlation of more complex phenomena, more representative of in-service conditions.

2. Materials and Methods

a. Experimental process

Rods from the same batch of 625 Ni-base superalloy were used for all the experiments carried out in this study. Their composition is given in *Table 1*. It can be noticed that the alloy contains low amounts of Mn in order to limit the formation of Mn-rich spinel on top of the oxide scale which could influence the volatilization phenomenon [1]. The samples consisted of disc-shaped coupons of 12 mm in diameter and 1.5 mm in thickness. Considering that the surface of the coupons directly influences the volatilization rate and thus the volatile species content of the gas mixture, a deviation of a maximum 5 % of the dimensions was allowed between samples. A hole of 2.5 mm was drilled at the very center of each specimen in order to allow the insertion of alumina rods necessary for sample positioning. Before oxidation tests, the samples were ground with SiC paper to a P600 grit surface finish and cleaned in ultrasonic bath with ethanol.

Table 1 Chemical composition of the Inconel 625 Ni-base superalloy investigated in at%. The analyses were made by EDS.

Element	Ni	Cr	Fe	Mo	Nb	Al	Si	Ti	Mn
at%	60.7	26.5	4.5	5.3	1.8	0.6	0.3	0.2	<0.1

All experiments consisted in isothermal oxidations carried out at 900 °C and under atmospheric pressure. A first test was conducted for approximately 500 hours in a furnace under quasi-static laboratory air and will be considered as the reference for the present study. All other oxidations were performed in a specific horizontal furnace allowing the control of the water

vapor content of the flowing gas mixture, as illustrated in *Fig. 1*. The volumetric inlet flows of O_2 and N_2 were independently managed thanks to gas flow controllers. The furnace consisted in an alumina tube with an inner diameter of 55 mm and a length of 1200 mm, heated by a three zones furnace. The wall's temperature profile was precisely measured every centimeter along the tube under a N_2 gas flow of 200 sccm (standard cm^3/min), using a K-type thermocouple with an accuracy of ± 2 °C. The settings applied allowed an isothermal zone 20 cm long with a temperature of 900 ± 5 °C between 49 and 69 cm from the inlet.

The atmosphere for wet oxidation tests consisted in a 74%N_2-18.5%O_2-7.5%H_2O (vol%) gas mixture (called wet flowing air thereafter). The wet gas was generated by passing a mixture of nitrogen and oxygen through a thermostated water saturator. The temperature of the distilled water in contact with the gas mixture was set at about 10 °C higher than that required to produce the nominal p_{H_2O}. The excess water vapor was subsequently condensed by cooling the wet gas in a distillation column. The temperature of the column was set so that the excess water vapor was entirely condensed in the distillation column, ensuring a water vapor content of 7.5 vol%. All pipes from the humidifier up to the furnace inlet were heated thanks to heating cords at 70 °C in order to avoid water condensation. A condenser placed at the outlet of the furnace allowed to check that the required water amount was maintained during the tests. According to preliminary CFD calculations carried out on FLUENT Ansys®, an inlet flow of 200 sccm was chosen to ensure a homogeneous flow around each sample. Tests with a flow rate of 500 sccm were also carried out to confirm the relevance of the approach.

Three samples spaced as described in *Fig.1* were placed in an alumina sample holder in the isothermal zone of the furnace for oxidation durations of 500 h. In the following, the specimens will be designated as *Upstream, Central* and *Downstream*, according to their position in the furnace. Complementary temperature measurements were made using K-thermocouples welded on three similar samples under a 200 sccm N_2 flow in order to check that all samples reached 900 °C.

For all oxidation experiments, the samples were regularly removed from the furnace and cooled to room temperature before being weighted on a microbalance with an accuracy of 20 µg. A maximum of 1 h was taken to make these measurements after what the samples were directly reinserted in the hot zone.

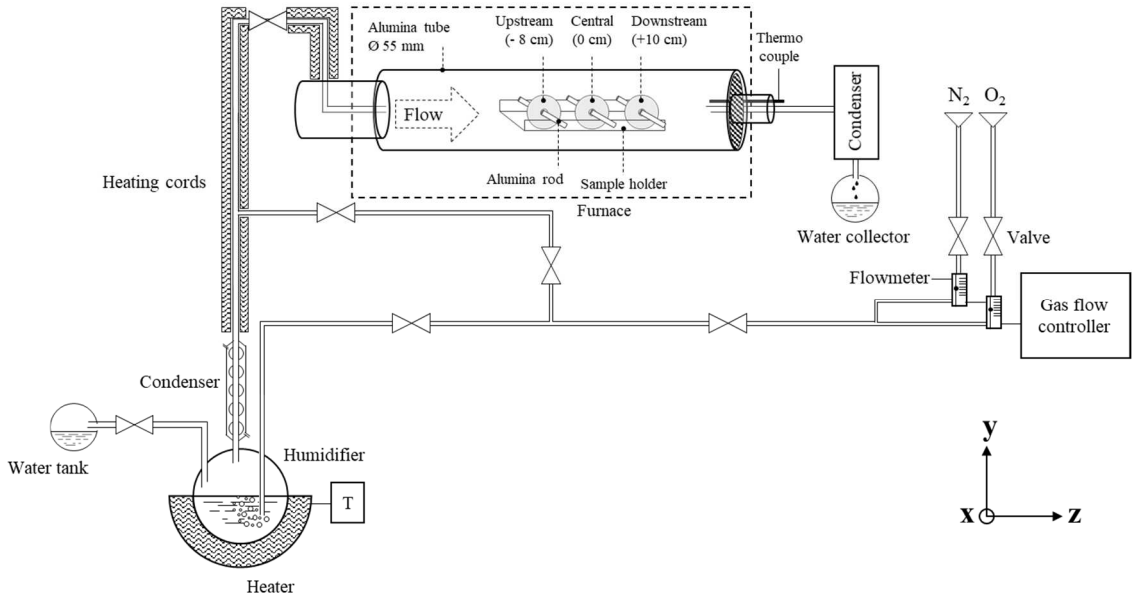

Figure 1 Schematic representation of the setups used for oxidation tests in flowing 74%N_2-18.5%O_2-7.5%H_2O.

The oxide scale phases were analyzed thanks to X-ray diffraction (XRD) using a Bruker D8 Discover diffractometer equipped with a copper source. The measurements were performed at room temperature with a θ-θ mounting, from 20° to 120° (in 2θ, with a step of 0.05° for an acquisition of 8 s per step).

The surface and cross section of the oxidized samples were observed by scanning electron microscopy (SEM) with a FEI Quanta 450 microscope using secondary electron (SE) and backscattered electron (BSE) modes.

The thickness of the oxide scales formed was measured using ImageJ on at least 6 SEM images with a systematic method. A threshold was applied to isolate the Cr_2O_3 scale which appeared in dark grey in BSE mode. Its surface area was then measured. It was thus possible to estimate its average thickness by dividing the area by the length. The measurement errors

related to the irregularity of the oxide morphology were then considered to be similar on all samples, making them comparable.

A Bruker Quantax EDS detector was used to determine the composition of the oxide scale and to measure Cr depletion from the alloy/oxide interface to the core of the samples.

b. Process simulation

i. Model description

A CFD model was developed to simulate the transport phenomena existing in the gas phase and the formation of $CrO_2(OH)_2$ according to *Reaction 1*. The numerical simulations were run using the computer design software, mesh generator and CFD code FLUENT ANSYS® 18.2. This code is a pressure-based, implicit Reynolds Averaged Navier Stokes solver that employs a cell-centered finite volume scheme having second-order spatial accuracy. It discretizes any computational domain into elemental control volumes, and permits the use of quadrilateral or hexahedral, triangular or tetrahedral and hybrid meshes. The local gas flow and temperature profiles were calculated by solving the mass and momentum conservation and thermal energy balance equations in each elementary discretized volume. The local distribution of species mass fractions and local vaporization reaction rates were calculated by solving the species conservation equations and the procedure detailed below.

Several assumptions were made to simplify the calculations:

- Steady-state conditions;
- Laminar gas flow, consistent with Reynolds number < 1000;
- Ideal gas;
- Incompressible gas flow due to the low Mach number < 0.04 in the furnace.

The physical properties of O_2, N_2 and H_2O were calculated from the FLUENT database using the kinetic theory of gases. For $CrO_2(OH)_2$, data to calculate the Lennard-Jones parameters were not available and thus, mean values close to that used by Young et al. [32]

were considered (collision diameter σ (equal to 4.5 Å) and characteristic energy of interaction ε (with ε/k equal to 340, k being the Boltzmann's constant).

The reactive area, the inlet pipe and the section reductions of the outlet, as they can presumably influence the gas flow, were represented by a three-dimensional (3D) geometrical domain of 2,213,966 hexahedral and tetrahedral cells. A refinement of the mesh was made around the samples and the substrate holder with a cell size of 300 µm. Taking advantage of the symmetry along the vertical symmetry plane (YZ plane on *Fig.1*), only half of the furnace was simulated.

The following boundary conditions were considered:

- A mass flow of 200 sccm was fixed at the gas inlet, corresponding to the experimental value. The gas temperature at the inlet and the wall temperature in the inlet pipe were respectively set equal to 70 and 96 °C, corresponding to experimental measurements. All species inlet mass fractions were fixed to the experimental values.
- A classical no-slip condition was applied for the gas velocity on the solid surfaces: walls, substrate surfaces, sample holder and alumina rods. A User Defined Function (UDF) was used to impose the temperature profile experimentally measured on all the walls, except on the samples on which the temperature was set at 900 °C as experimentally measured.
- The mass flow density of each species (except N_2) on the sample surface was calculated from the volatilization rate detailed below and the stoichiometric coefficients of *Reaction 1*. On all other surfaces, which are in inert alumina, these mass flows were considered as zero.
- At the exit, a pressure outlet boundary condition was applied. The total pressure was fixed at the operating pressure, equal to atmospheric pressure (101 325 Pa). A zero-diffusion flow was applied to all other gas phase variables at the exit.

The volatilization reaction was implemented into FLUENT as a surface reaction. It was quantified thanks to a second UDF. Only the phenomena represented by *Reaction 1* were considered, assuming that the surface of the samples was rapidly fully covered by Cr_2O_3 and thus that the chromia scale formation was not rate-limiting. Indeed, experimental tests and calculations were carried out in the regime of chromia scale growth before reaching significant Cr-depletion in the metallic alloy. Several authors showed that for high enough amounts of Mn and Ti, spinel and Ti-rich oxide could form on top of the oxide scale of chromia-forming alloys. This is known to shield the volatilization of Cr_2O_3 considered in the CFD model. However, in the present study, microstructural observations and oxide scales characterization by XRD and EDS allowed to consider these oxide formation as negligeable in a first approximation (as detailed in section *3.b.ii* below). The diffusive transport of the volatile species from the surface was supposed to be the rate-limiting step. So, the rate of the volatilization reaction was assumed to be equal to the diffusive flux leaving the sample surface. The diffusion of $CrO_2(OH)_2$ in the flowing gas mixture was quantified by the Fick's law (*Equation 1)*. The aim was to take into account the reduced driving force for the volatilization due to the enrichment of the atmosphere with $CrO_2(OH)_2$ (*Reaction 1)*, as discussed by Holcomb *et al.* [1] and done by Jacobson *et al.* [14]:

$$J_{CrO_2(OH)_2} = \frac{D_{CrO_2(OH)_2}}{dRT}\left(P^{S}_{CrO_2(OH)_2} - P^{\infty}_{CrO_2(OH)_2}\right) \qquad \text{(Equation 1)}$$

Where $J_{CrO_2(OH)_2}$ is the flux density of $CrO_2(OH)_2$ (in $mol.m^{-2}.s^{-1}$), $D_{CrO_2(OH)_2}$ is the diffusion coefficient of $CrO_2(OH)_2$ in the gas mixture (in $m^2.s^{-1}$), d is the characteristic length used by Fluent to calculate diffusive fluxes (in m) and $P^{S}_{CrO_2(OH)_2}$ and $P^{\infty}_{CrO_2(OH)_2}$ stand for the partial pressures of $CrO_2(OH)_2$ respectively close to the surface and in the free gas (in Pa). The partial pressure of $CrO_2(OH)_2$ close to the substrate surface was assumed to be equal to its equilibrium pressure ($P^{S}_{CrO_2(OH)_2}$) calculated by *Equation 2*.

$$P^{S}_{CrO_2(OH)_2}(atm) = a^{1/2}_{Cr_2O_3} P_{H_2O} P^{3/4}_{O_2} exp\left(-\frac{\Delta G^o}{RT}\right) \quad \text{(Equation 2)}$$

In this expression, $a_{Cr_2O_3}$ stands for the activity of Cr_2O_3 (set equal to 1, considering that no other oxide compete with Cr_2O_3), P_{H_2O} and P_{O_2} are the partial pressures of H_2O and O_2 respectively (in Pa), ΔG^o is the standard Gibbs energy of Reaction (R1) (in J.mol^{-1}), R the gas constant (in J.mol^{-1}.K^{-1}) and T the temperature (in K). The standard Gibbs energy was estimated using the thermodynamic calculations of the reaction enthalpy and entropy of Opila *et al.* [16] with T in K (*Equation 3*):

$$\Delta G^o = 53500 + 45.5T\ (J/mol) \quad \text{(Equation 3)}$$

So, in *Equation 1*, the flux density and the $CrO_2(OH)_2$ partial pressure in the free gas are unknown. The implementation of the UDF avoids any fitting of the kinetics because the flux density is calculated in a first step thanks to the UDF, then FLUENT can estimate partial pressures. As for all unknown parameters, FLUENT used an iterative procedure to adjust their values up to convergence.

ii. Methodology of comparison between experimental and simulation results

Using the simulation results, the $CrO_2(OH)_2$ fluxes released from the coupon surfaces were calculated, allowing to obtain CFD volatilization constants (k_v') values. It is worth noting that as *Equation 1* is based on several questionable assumptions previously described, one of its parameters was adjusted to better represent the experimental volatilization constants. Indeed, in this equation, the Cr_2O_3 activity and the Gibbs energy values are not well established. Concerning the first parameter, the oxide scale formed was mainly Cr_2O_3. Reducing the activity of the oxide would therefore not have been consistent. Holcomb *et al.* [6] reminded in their study, this parameter was not well established for $CrO_2(OH)_2$ justifying an adjustment. Initially, ΔG^o was set to 107 kJ.mol^{-1} according to Opila *et al.* [16] study. By comparing the values obtained by CFD and from experiments, we found that a better fit was reached for 100 kJ.mol^{-1}.

For comparison with the simulation results, experimental data extracted from the mass variation curves of the oxidized 625 alloy were used to determine the parabolic oxidation constant k'_p and the volatilization constant k'_v on different samples. This was done using *Equation 4* that describes the global mass variation kinetics and considering no variation of the samples surface along the oxidation tests. In this expression, *m* is the mass of the sample per unit area (in mg.cm^{-2}), m_O is the oxygen mass gain per unit area due to Cr_2O_3 formation (in mg.cm^{-2}), *t* is the time (in s). Despite years of studies [3,7–9,14,16,32], no mathematical solution was found to *Equation 4* making it difficult to directly determine a value of volatilization constant k'_v from the experimental data. Thus, a numerical fit of the mass variations was proposed to approximate the experimental volatilization rate.

$$\frac{dm}{dt} = \frac{k'_p}{2m_O} - k'_v \qquad \text{(Equation 4)}$$

3. Results and discussion

a. Preliminary tests – volatilization highlighting

Preliminary tests were carried out in the tubular horizontal furnace at 900 °C with a flowing wet air of 200 sccm. *Fig. 2a* shows the mass variations of the three samples as a function of their position in the furnace after 72 h of exposure. Also, the mass variations obtained after 72 h in quasi-static laboratory air is given as a reference.

Two striking points were highlighted by this test. The first one is the low mass variations of the samples oxidized in the presence of water vapor compared to the reference (whose mass gain was equal to 0.42 mg.cm^{-2} after 72 hours of exposure). The second, is the significant increase in the mass gain from the Upstream to the Downstream sample. Considering that all three samples were taken from the same batch, underwent the same surface preparation and were located in the isothermal zone of the furnace, this result was not expected in a first approach.

A complementary test was carried out in order to ensure that the mass variation differences were not related to the samples themselves. The same three oxidized samples were exposed again for an additional 72 hours duration to similar oxidizing conditions. However, the Upstream sample was placed Downstream and conversely. Only the Central specimen was placed at the same position than in the first 72 hours. The mass variations measured after the second run of 72 h are reported in *Fig. 2b*. It can be noticed a decrease in the mass change of the Upstream sample which showed the highest mass gain after the first 72 hours of exposure at the Downstream position. On the contrary, the Downstream sample which showed the lowest mass gain after the first run of 72 hours (at the Upstream position) showed a strong increase in its mass during the second run.

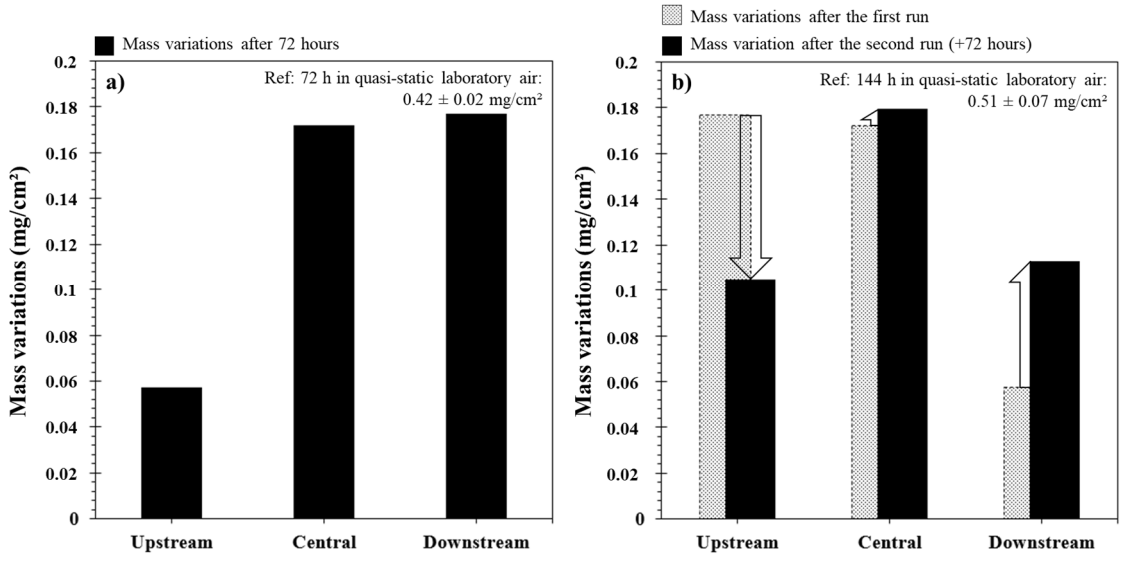

Figure 2 Influence of the sample position on the mass variation of the 625 alloy exposed at 900 °C and P_{atm} in 74%N_2-18.5%O_2-7.5%H_2O flowing at 200 sccm: a) after the first run of 72 hours and b) after the second run of 72 hours following the switch of the Upstream and Downstream samples. The mass variation references measured after 72 hours (a) and 144 hours (b) of oxidation in quasi-static laboratory air are given as reference.

This couple of experiments was the starting point of the present study. Firstly, the lower mass gains of the samples exposed to flowing 74%N_2-18.5%O_2-7.5%H_2O compared to the reference in quasi-static laboratory air highlighted the important volatilization of the chromia scale, as observed in several works [5,32,36,37] and as expected considering *Equation 4.*

Secondly, the heterogeneity of the mass variations for the first 72 h of exposure suggested an eventual influence of the sample position on the oxidation behavior, and more specifically on the volatilization rate. The important mass changes measured on the Upstream and Downstream specimens after their position change for the second 72 h test confirmed the influence of the sample position on the volatilization kinetics.

All parameters being similar for the three samples, the main hypothesis proposed to explain these differences was a change in the gas mixture composition, more specifically an enrichment of the gas flow in $CrO_2(OH)_2$ volatile species. As described by *Equation 1*, the $CrO_2(OH)_2$ flow leaving the oxide scale surface should be reduced by an increase in the $CrO_2(OH)_2$ partial pressure of the environment. Therefore, a gas mixture enriched in volatile species arriving at the surface coupon would slow down the volatilization rate. This phenomenon was evocated by Holcomb *et al.* [1] as one possible way to mitigate the volatilization of the chromia scale.

The main consequence of this slowing down of the volatilization from the Upstream to the Downstream could lead to large oxidation kinetics differences along pipes crossed by oxidizing and water vapor-rich gases, with a higher degradation in the Upstream areas. From an experimental point of view, this means that the three aligned samples along the flow direction should not be considered as if they underwent similar environments. Their oxidation kinetics cannot be used together to determine a mean value as if they were the repeatability samples of one unique test. In an industrial point of view, this suggests that a pipe crossed by a flowing oxidizing hot gas enriched in water vapor could show heterogeneous oxidation behaviors from entry to exit. In order to correctly interpret the results of oxidation in the presence of water vapor, the influence of the $CrO_2(OH)_2$ enrichment of the environment will be deeply investigated further down in the article.

b. Effects of water vapor

i. *Mass variations*

To complete the previous results, similar oxidation tests were carried out for longer durations. *Fig. 3* offers a comparison of the oxidation behavior of the 625-alloy exposed to quasi-static laboratory air and to flowing wet air for 500 h.

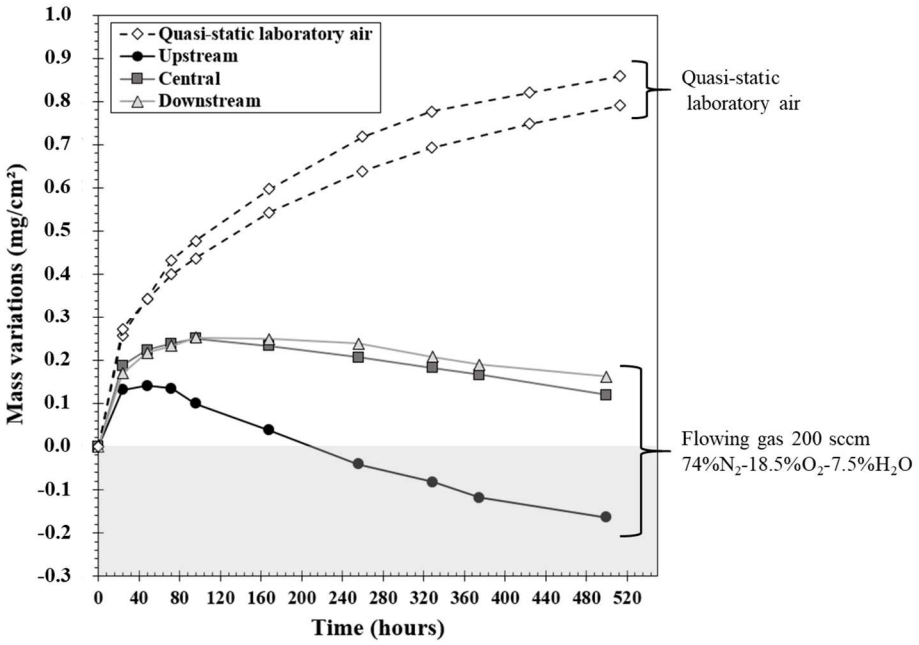

Figure 3 Mass variations versus time for 625 specimens oxidized for approximately 500 h at 900 °C in dry air in quasi-static laboratory air and in flowing 74%N_2-18.5%O_2-7.5%H_2O (Upstream, Central and Downstream samples).

Under quasi-static laboratory air, the mass variations follows a parabolic oxidation law (*Equation 5)* with a parabolic oxidation constant k_p equal to (5.1 ± 1.1) x 10^{-7} $mg^2.cm^{-4}.s^{-1}$. The gap noticed between the two curves shows the results dispersion. As a comparison, Buscail *et al.* [7,9] found a value of 3.2 x 10^{-7} $mg^2.cm^{-4}.s^{-1}$ for the 625 alloy oxidized at 900 °C in air containing 0.3 vol% H_2O for 48 h of exposure which is consistent with our results, especially considering that the laboratory air cannot be considered as dry.

$$\frac{\Delta m}{S} = \sqrt{k_p \times t} \qquad \text{(Equation 5)}$$

For the three samples exposed to flowing wet air, the mass variation curves (*Fig. 3*) show a mass increase up to a maximum depending on their relative position in the furnace, before decreasing according to a linear law until the end of the test.

This specific mass variation-curve shape is characteristic of an oxide scale growth controlled by diffusion trough the oxide scale combined to an oxide volatilization at a constant rate. The global lower mass variations compared to those measured in laboratory air were consistent with a competitive chromia-loss due to volatilization and the oxygen gain to form the chromia scale, following a law represented by *Equation 4*. After the transient stage, the chromia scale thickening slows down, in agreement with an oxidation kinetics controlled by diffusion across the oxide scale but also because of its volatilization, as described by *Equation 6*.

$$\frac{de}{dt} = \frac{k_p}{2e} - k_v \qquad \text{(Equation 6)}$$

Where e is the thickness of the oxide scale, t the time, k_p the parabolic oxidation constant in $cm^2.s^{-1}$, proportional to the diffusion coefficient in the oxide scale, and k_v the linear volatilization rate of the oxide scale in $cm.s^{-1}$.

Equation 6 shows that the growth rate of the scale is decreasing with the increase in the scale thickness to eventually reach a steady state when the thickness approaches a limit value, e_L, as described by *Equation 7*.

$$\frac{de}{dt} = 0 \Rightarrow e_L = \frac{k_p}{2k_v} \qquad \text{(Equation 7)}$$

The mass gain thus slows down and decreases as the oxide scale grows until e_L is reached. When the steady state is reached, the oxide scale thickness is constant but the sample is losing a mass corresponding to the Cr lost by volatilization.

Fig.4 also confirms the results of the preliminary tests, namely, the influence of the relative position of the samples on their oxidation behavior. The Upstream coupon showed a maximum weight gain (0.14 $mg.cm^{-2}$) after only 72 hours and then reached a linear steady-state. This sample underwent negative mass variations after 200 h of exposure. As a comparison, the Central and Downstream coupons reached a higher maximum weight gain (0.245 $mg.cm^{-2}$) after 96 h and their kinetics of mass loss during the steady state was slower. Only slight differences

were noticed between the Central and the Downstream samples, which behaviors can be considered as very similar knowing the measurement dispersion.

Since no analytical solution of *Equation 4* exists, it was solved numerically with an incremental calculation. This numerical solution of the net mass change as a function of time was fitted to the experimental data. In the proposed approach, k_p' and k_v' were modulated to fit a mass variation curve based on *Equation 4* with the experimental data obtained for each sample. It was thus possible to approximate the values of both constants. When doing these fits, it was found that the curve fitting for the first 20 h was not perfect. This was attributed to an initial oxidation regime with faster oxidation kinetics, as often encountered with Ni-base superalloys. As shown by *Equation 4*, the initial mass gain (when m_O is small) is mostly due to diffusion (k_p'). The variations during the transient regime affected the fitted value of k_p' which in turn affected the fitted value of the volatilization parameter k_v'. Therefore, it was decided to fit the mass change curves between 20 and 500h and with a unique common value of k_p' for all three coupons. This value of k_p' corresponds to the growth of the oxide scale when there is no oxide volatilization. Moreover, it can be experienced that if the values of k_p' and k_v' are modified by 10% for the Upstream sample and 3% for the Central and Downstream ones, the quality of fits is severely degraded. This allows to define the precision of the obtained values (one example is given in *Fig. 10b*).

The determined values summarized in *Table 2* show a decrease in the k_v' values from the Upstream sample to the Downstream one. This is consistent with the preliminary experiments and confirms the hypothesis of a larger volatilization rate occurring at the Upstream coupon surface compared to the next coupons. It can be argued that when the flowing gas met the Central and then the Downstream samples, the environment was not only 74%N_2-18.5%O_2-7.5%H_2O. It also contained $CrO_2(OH)_2$ due to its formation at the Upstream coupon surface. This $CrO_2(OH)_2$ enrichment of the gas phase would then lead to a decrease in the Cr-volatilization and thus in the lower mass loss of the Central and Downstream samples,

according to *Equation 1*. Finally, the fact that no significant difference was noticed between the last two samples suggests that the volatilization reaction at the Upstream sample surface sufficiently increased the $CrO_2(OH)_2$ amount to considerably decrease the volatilization rate on the following samples and that, in comparison, the contribution of the Central sample to the volatile species enrichment of the gas flow was negligeable. This phenomenon will be more deeply investigated below in the article.

Table 2 Values of k'_p and k'_v estimated by numerical fit based on the experimental data. The standard deviation of the k'_v values were determined by modulating k'_v values to make the numerical fit surround the experimental mass variation curves.

Position	k'_p (mg².cm^{-4}.s^{-1})	k'_v (mg.cm^{-2}.s^{-1})
Upstream	2.83 x 10^{-7}	(4.5 ± 0.5) x 10^{-7}
Central	2.83 x 10^{-7}	(2.85 ± 0.1) x 10^{-7}
Downstream	2.83 x 10^{-7}	(2.6 ± 0.1) x 10^{-7}

ii. *Scale morphology and composition*

Fig. 4 shows SEM micrographs of alloy 625 coupon surfaces exposed to quasi-static laboratory air and to flowing wet air. A dense Cr_2O_3 scale was observed on all samples and only slight differences were highlighted. The chromia scale grown in quasi-static laboratory air (*Fig. 4a*) appeared to be a bit denser than in the presence of water vapor where a more granular structure with more pronounced Cr_2O_3 grain boundaries was observed (*Fig. 4b, 4d, 4e*).

Fig. 4c shows a magnification of the Upstream coupon surface after 500 h of oxidation under the flowing wet gas. Whiskers were observed all over the surface and their density decreased from the center of the disc-shaped sample to the external edges. This specific blade-shaped growth of Cr_2O_3 is frequently reported when water vapor is present among the oxidant gases [38–41]. In their review, Saunders *et al.* [3] explained that the mechanism for whiskers formation, at first discussed by Raynaud *et al.* [42], was related to the presence of dislocations in the oxide independently of the volatilization. Nguyen *et al.* [39] recently confirmed this

hypothesis by TEM observations of blade-shaped whiskers on a Fe-base alloy oxidized at 818 °C in an Ar-20%CO_2-20%H_2O mixture. They showed that the blade nucleation frequency increased with the surface roughness of the scale thickness, associated with a growth of the stresses in the oxide. Concerning the specific influence of the water vapor, they suggested that the formation of the whiskers was related to a faster dissociation of water molecules at the tip of the blades, favoring their growth [42].

In the current study, the presence of blades on the Upstream sample only would thus suggest that this latter underwent a stronger influence of the water vapor. This would be consistent with the mass variation curves which showed that the Upstream sample was more susceptible to volatilization. The condenser placed at the exit of the furnace allowed to measure the water volume after the reaction with the samples. No significant water loss was measured in the gas mixture after crossing through the furnace. This confirms that only a negligible amount of water vapor was consumed by the Upstream sample. Moreover, considering *Equation 2*, a maximum oxyhydroxide partial pressure of 3.64×10^{-7} atm should be formed at the coupon surface, which should lead to only small changes in the water vapor partial pressure. As a consequence, the water vapor reaction with the Upstream sample cannot explain why whiskers were not observed on the oxide of the Central and Downstream samples. It is possible that the surface morphology of Cr_2O_3 at the surface samples could be impacted by the volatilization phenomenon and not only by the presence of water vapor in the gas phase. Indeed, the presence of $CrO_2(OH)_2$ in the gas phase flowing over the Central and Downstream samples could influence and potentially limit the water vapor adsorption at their surface and thus the formation of whiskers. The presence of these whiskers could influence the volatilization rate on the Upstream sample surface by significantly increasing the reactive surface as compared to the Central and Downstream samples.

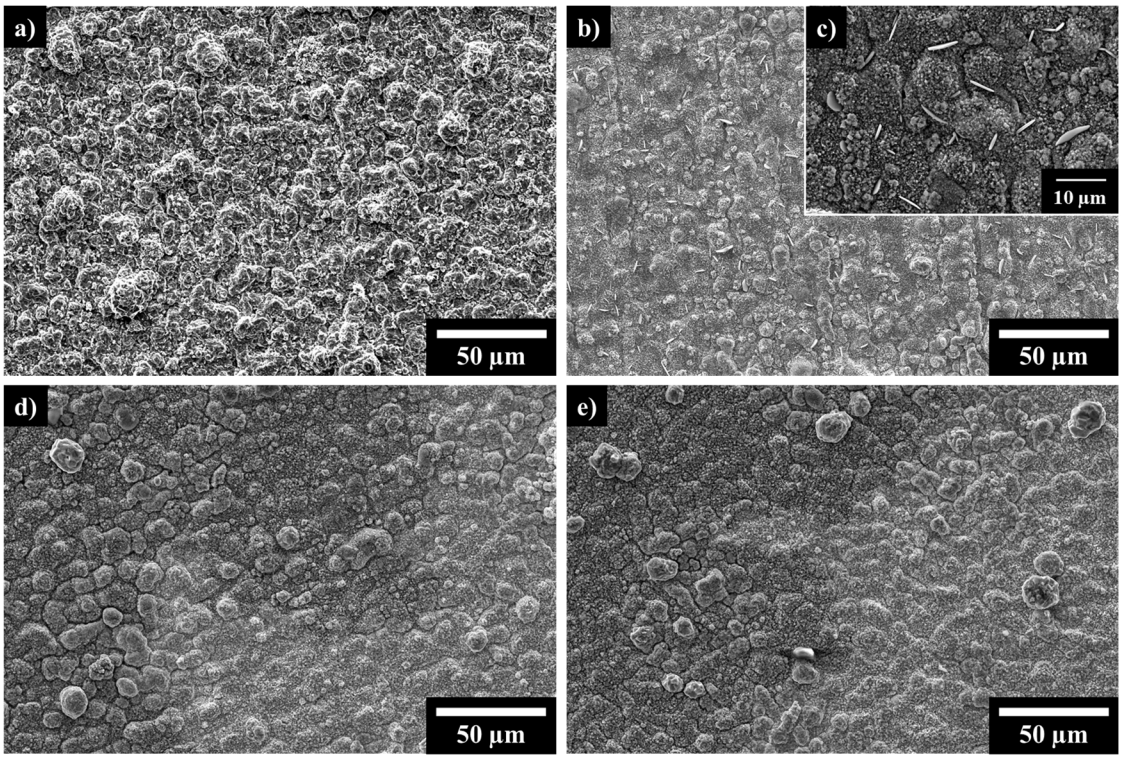

Figure 4 SEM images of alloy 625 surface after 500 hours of oxidation at 900 °C in quasi-static laboratory air (a) and under flowing 74%N_2-18.5O_2-7.5%H_2O: b) and c) Upstream, d) Central and e) Downstream.

The XRD spectra in *Fig. 5* confirm that the oxide scale formed on the sample surface was mainly composed of Cr_2O_3, independently of the environment considered. This was also true on the Upstream sample, confirming that the whiskers had a composition similar to the oxide scale. Moreover, the Cr_2O_3 peaks showed similar intensities without and with water vapor suggesting that the presence of water vapor did not modify the crystallographic texture of the oxide.

These analyses also highlighted the presence of the δ-Ni_3Nb phase as classically observed during the oxidation of the 625 alloy. Chyrkin *et al.* [33] explained this phenomenon by an uphill diffusion of Nb due to a decrease in the Nb activity in the Cr-depleted zone below the oxide scale. As a consequence, a thin layer of Ni_3Nb formed directly beneath the Cr_2O_3 scale, as confirmed by SEM and EDS analyses and shown for the Upstream sample in *Fig. 6.* The latter details only the results concerning the Upstream sample. Indeed, all other samples, whatever the environment and position, show a very similar microstructure. These observations

confirmed XRD results and allowed to implement the discussion about the oxide scale. Indeed, in *Fig.6*, local Ti-enrichments were highlighted in the oxide scale, with a mean amount of 0.8 at% (based on 8 measurements) and a maximum of 1.2 at% measured by EDS with quantitative method. Although it was not directly observed or detected by XRD, this suggests that Ti-rich oxide may have formed at the scale surface in very small amounts or might form for longer exposure durations. Titanium nitrides were also observed in the matrix in *Fig.6* as expected according to the literature review [43–45]. Concerning the Mn amounts, it is known that chromia forming alloys containing more than 0.3 wt% of Mn may form spinel rich in Mn and Cr (e.g. $MnCr_2O_4$) [46]. The spinel forms at the gas/oxide interface which is explained by the fast outward diffusion in Mn through Cr_2O_3 at 900 °C compared to Ni or Cr as shown by Lobnig *et al.* [47] who measured the diffusion coefficients of various elements including Mn in pure chromia. The low amounts of Mn measured in the 625-alloy used in this study can explain why no spinel was observed. In very similar experimental conditions, several authors draw the same conclusions on 625 alloys [7,17]. Quantitative EDS analyzes were carried out to measure the Mn amount in the oxide scale and showed a mean value of 0.4 at% (based on 8 measurements) and a maximum value of 0.5 at%. However, these results must be considered carefully. Indeed, the EDS analyses accuracy is of 0.5 at% for Mn and the Kα of Mn (5.900 keV) intersect the Kβ of Cr (5.947 keV). A last observation with SEM-EDS was the precipitation of aluminum oxide along the grain boundaries below the oxide/alloy interface, as frequently observed in 625 alloy [48].

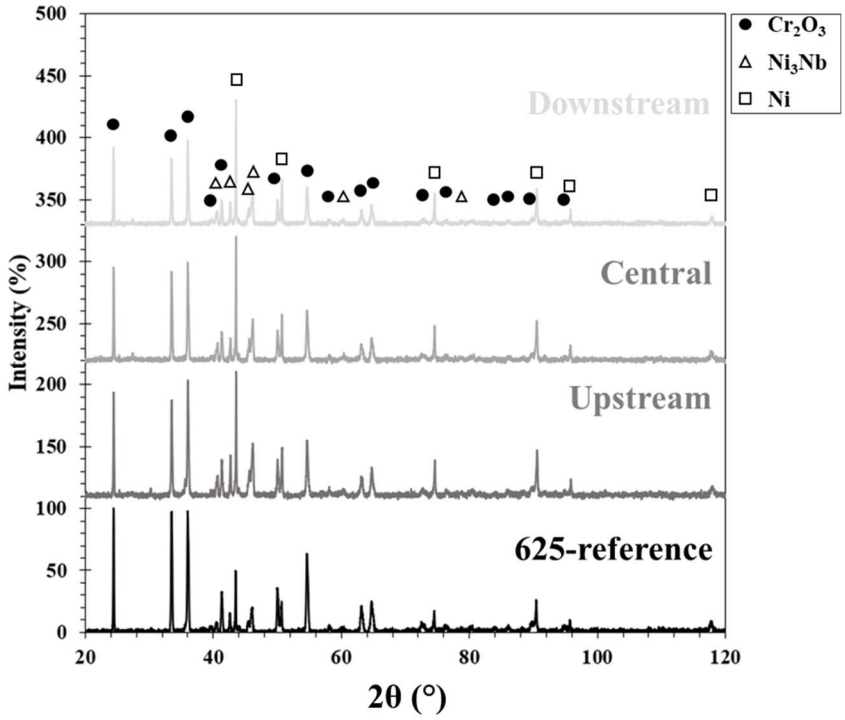

Figure 5 XRD measurements after 500 h oxidation of the 625 alloy at 900 °C in quasi-static laboratory air (Reference) and under wet flowing air (Upstream, Central, Downstream). (●: Cr_2O_3 / Δ: Ni_3Nb / □: Ni)

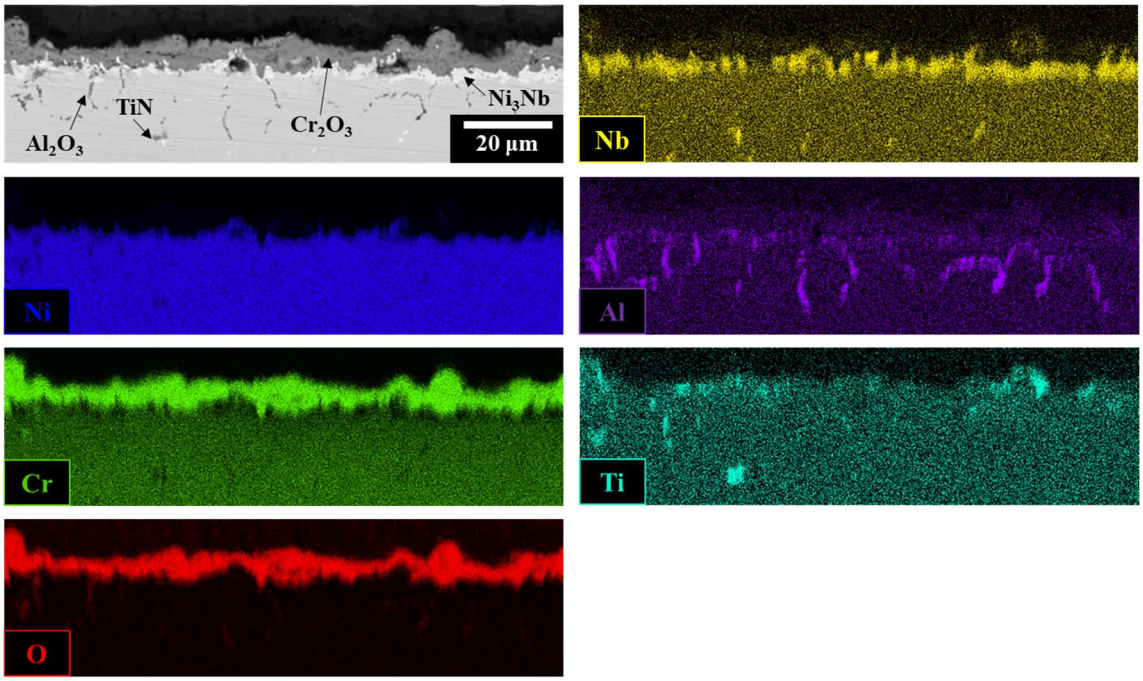

Figure 6 Cross section of alloy 625 (at the Upstream position) after 500 h of oxidation at 900 °C in 74%N_2-18.5%O_2-7.5%H_2O observed by SEM in BSE mode and analyzed by EDS.

Based on SEM observations, the thickness of the Cr_2O_3 scale after 500 h of oxidation in quasi-static laboratory air and in flowing wet air was measured and values are summarized in *Table 3*. For the reference sample exposed in laboratory air, the measured oxide thickness corresponds to the continuous growth of Cr_2O_3 which is not the case for the three samples oxidized in the water vapor enriched gas flow. Indeed, for these lasts, as previously explained, at this stage, the steady-state was reached. Thus, the thickness of the oxide scales which was measured corresponded to e_L *(Equation 7)*. Table 3 shows that the presence of water vapor led to a decrease in the oxide thickness compared to the sample tested in laboratory air. This is consistent with a slowdown of the oxide growth kinetics due to the volatilization, according to *Equation 6.* Moreover, e_L was shown to be smaller at the Upstream coupon surface than for the Central and the Downstream samples. This was also expected, considering *Equation 7*, which defines e_L as only dependent on k_p and k_v, and the fact that k_v' was higher on the Upstream sample than on the other ones (*Tables 2* and *3*). Such evolution of the oxide scale thickness in the presence of water vapor was also noticed on Ni-25Cr alloys exposed at 1000 °C in air+80%H_2O [37] and in air with 180 mbars H_2O [49]. In both cases, the presence of water vapor during high temperature oxidation was shown to enhance chromia volatilization. The evolution of the oxide scale thickness between the three samples tends to confirm that the Upstream coupon underwent an environment favoring more volatilization than the two others.

Table 3 Comparison of the Cr_2O_3 scale thickness on the reference 625 alloy oxidized 500 h in quasi-static laboratory air at 900 °C and the 625 Upstream, Central and Downstream samples oxidized 500 h in flowing 74%N_2-18.5%O_2-7.5%H_2O. The measurements were carried out using the ImageJ software.

Samples	**Experimental Cr_2O_3 thickness (µm)**	**e_L (µm) calculated from Equation 7**
Reference	6.5 ± 0.9	-
Upstream	4.3 ± 0.3	4.1
Central	5.2 ± 0.2	6.5
Downstream	5.0 ± 0.4	7.2

iii. Chromium depletion

The last studied parameter was the influence of the volatilization during oxidation on the Cr depletion under the oxidized surfaces. *Fig. 7* shows EDS profiles of Cr atomic composition of samples exposed in quasi-static laboratory air and in flowing wet air. The profiles were obtained from the bulk oxide scale to the core of the specimen. The Cr-depletion was shown to decrease from the Upstream to the Downstream sample, this latter having a Cr-profile close to the sample exposed in laboratory air. This result is consistent with previous observations: the faster volatilization rate on the Upstream sample implies a larger Cr-depletion to maintain the Cr_2O_3 scale. The increased Cr-depletion was observed before by Young and Pint [32] on thin foils of alloy 709 exposed 5000 h in air + 10%H_2O at 800 °C. In their study, they performed complementary calculations which allowed a comparison between the Cr mass loss and the Cr mass used for the Cr_2O_3 growth and the $CrO_2(OH)_2$ volatilization.

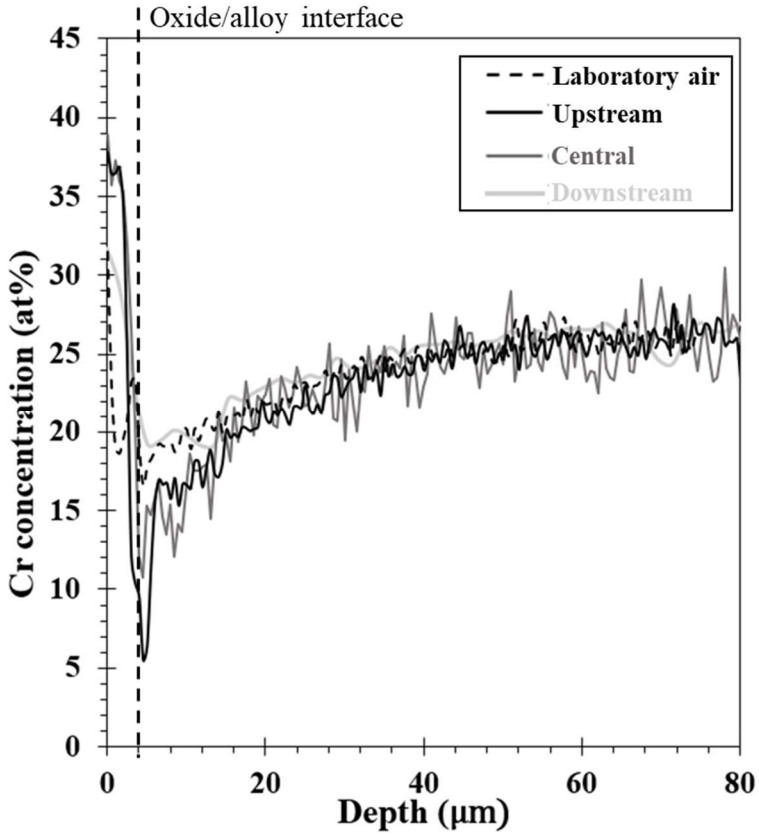

Figure 7 Variations of the Cr atomic percent from few µm of the alloy/oxide interface to the bulk alloy measured by EDS in coupons oxidized 500 h at 900 °C in quasi-static laboratory air and in flowing 74%N_2-18.5%O_2-7.5%H_2O mixture

c. CFD calculations

The aim of the CFD simulations using FLUENT Ansys® is to analyze the consistence of the hypotheses previously drawn on the volatilization process and the influence of the gas phase composition changes on the sample oxidation behavior.

All the simulation results are plotted along the vertical symmetry plane of the furnace. *Fig. 8a* shows the gas velocity profile in the whole furnace. The highest velocities (max. 1.1 $m.s^{-1}$) were logically observed in the inlet and outlet tubes, corresponding to zones of reduced section area for the gas flow. In *Fig. 8a* the maximal value of the scale was set to 1.8 x 10^{-1} $m.s^{-1}$ in order to better display velocity variations around the samples. Recirculation loops are visible in the 20 first cm near the inlet, due to the offset position of the inlet tube. They do not influence

the gas flow behavior in the isothermal area where the oxidation / volatilization reactions occur. Indeed, a parabolic profile is observed in the furnace before and after the sample's region, corresponding to a classical laminar flow behavior. The average velocity on a furnace section area logically increases with the gas temperature, due to the increase in the gas volume. *Fig. 8b* focuses on the gas velocity vectors evolution in the isothermal zone. The velocity profile appears to be very similar around the three samples independently of their position in the furnace, another time of parabolic shape. At 100 µm from the sample surfaces, the local gas velocity is close to $1.8.10^{-3}$ $m.s^{-1}$.

The temperature profile of the gas mixture in the whole furnace is provided in *Fig. 8c*. It follows the profile imposed on the furnace walls by the UDF thanks to high conductive and convective thermal transfer rates. The gas reaches the nominal temperature of 900 +/ -5 °C 5 cm before the samples zone, which appears to be isothermal at 900 ± 5 °C till 5 cm after the last sample. This explains why the gas velocity profile is similar around the three samples.

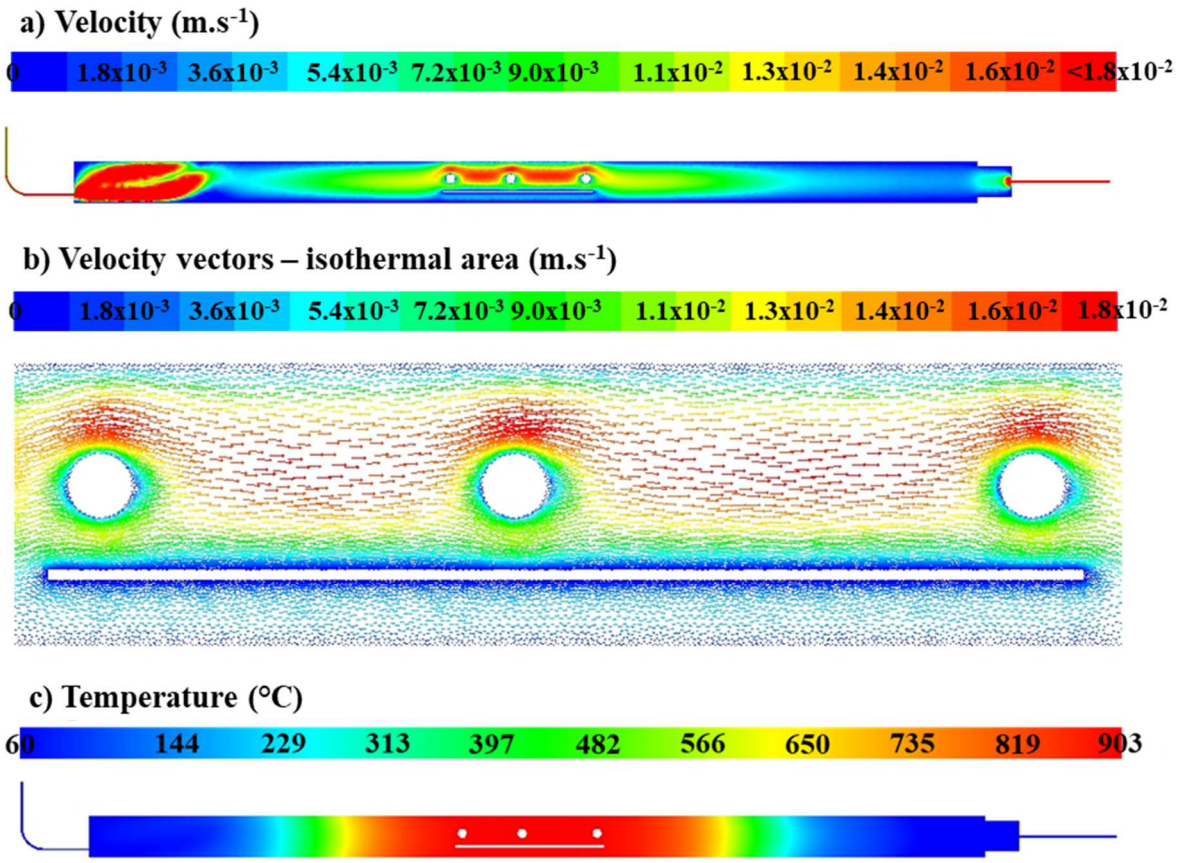

Figure 8 a) Gas velocity profile along the vertical symmetry plane of the furnace, b) Gas velocity vectors drawn in the isothermal zone around the three samples and c) Temperature profile along the vertical symmetry plane of the furnace. The gas flows from the left to the right.

Fig. 9 shows the evolution of the species molar fractions in the isothermal zone. For oxygen (*Fig. 9a*) and water vapor (*Fig. 9b*), a very slight decrease in their molar fraction is calculated along the furnace length in the samples zone, explaining the pixelated shape of the profiles. This decrease is due to the formation of $CrO_2(OH)_2$ in the gas phase and to the increase in its molar fraction while the reaction occurs on the sample surfaces (*Fig. 9c*). A maximum $CrO_2(OH)_2$ partial pressure of 3.6×10^{-7} atm was calculated at the sample surfaces, very close to the $CrO_2(OH)_2$ partial pressure at equilibrium expected from *Equation 2*. These low quantities of volatile species released from the samples surface explain why only slight changes were noticed for the molar fractions of O_2 and H_2O which are in excess (a difference of 5 orders of magnitude compared to $CrO_2(OH)_2$). These small changes are consistent with the fact that no

water consumption was measured in the water collector placed at the furnace outlet, as previously discussed. It can also be noticed that the molar fraction changes (approximately 10^{-4}%) in O_2 and H_2O occur 15 cm before the first sample, due to $CrO_2(OH)_2$ diffusion in the flowing gas.

More specifically, the CFD calculations show that even if the molar fraction of volatile species released is low, this is enough to modify the local gaseous environment around the samples with a flow rate of 200 sccm, which could explain the previous experimental observations. To better analyze this aspect, the $CrO_2(OH)_2$ molar fraction evolution along a line in the furnace axial direction is plotted at 100 µm from the coupons surface in *Fig. 9d.* A large increase in the $CrO_2(OH)_2$ mole fraction appears near the Upstream sample position which leads to a modification of the gas phase composition. The subsequent increases calculated near the Central and Downstream samples are much lower. This is consistent with a decrease in the driving force for the volatilization reaction for these two samples: according to *Equation 1,* the difference between the $CrO_2(OH)_2$ molar fractions at the samples surface and in the gas phase is reduced.

This influence of the gas enrichment occurring at the Upstream sample surface is thus significant on the behavior of the following samples. However, although this is true for low gas velocity, this behavior is expected to change for higher gas velocities more representative to in-service conditions as the volatilization rate is expected to be directly dependent to the flow rate. Indeed, Sand *et al.* [18] suggested that for low flow rates (considered as an equilibrium regime), the volatilization is proportional to the flow rate whereas for higher flow rates (>25 $cm.s^{-1}$ [50]), Cr volatilization may become independent of the flow rate when the volatilization kinetics is controlled by the reaction. Then, it may be expected that for high enough flow rates, the accelerated transport of $CrO_2(OH)_2$ from the samples surface can increase the volatilization rate on all samples. But due to the dilution effect, the differences between two samples will be reduced.

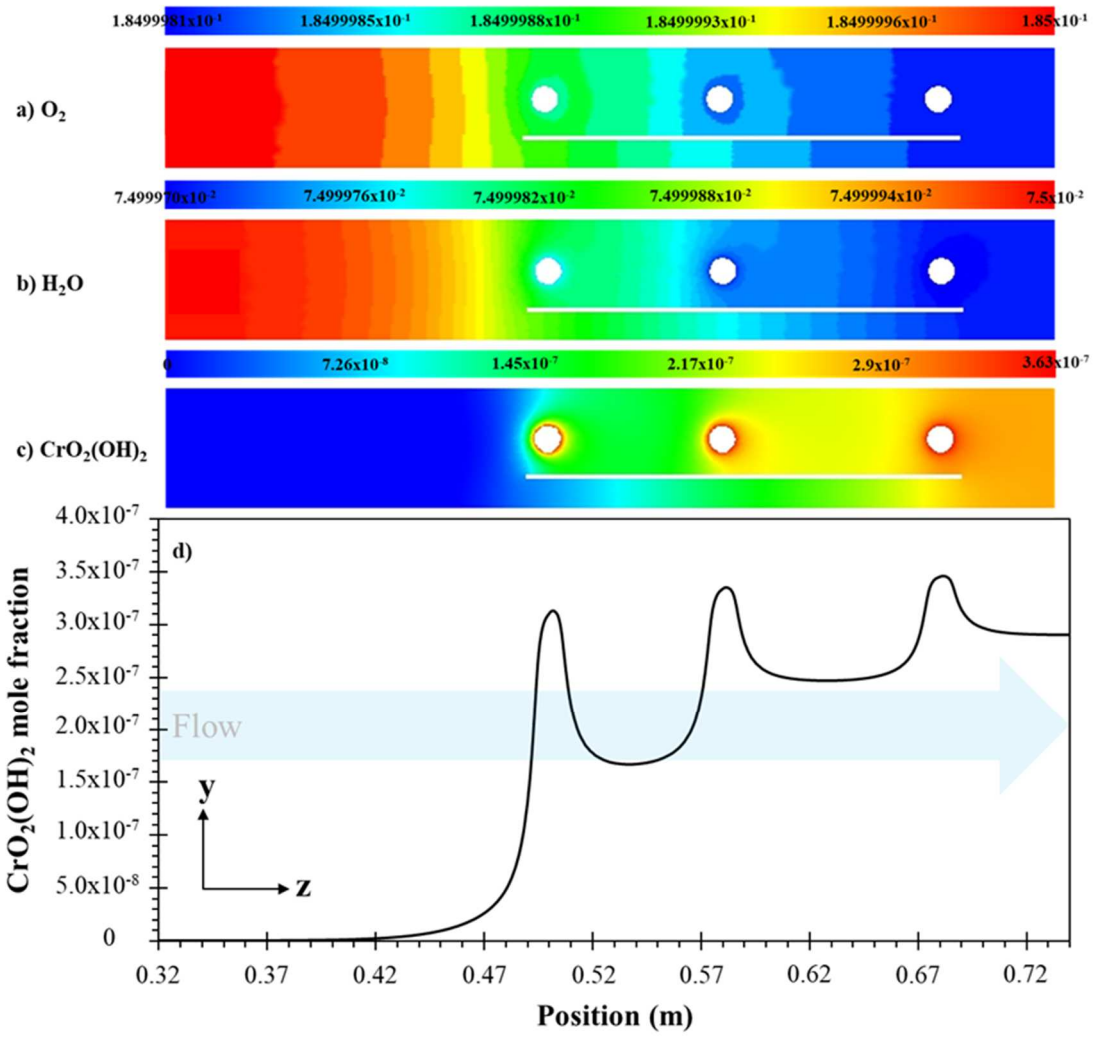

Figure 9 Gas species molar fraction profiles: a) O_2, b) H_2O, c) $CrO_2(OH)_2$. d) $CrO_2(OH)_2$ molar fraction evolution along a line in the furnace axial direction plotted at 100 µm from the coupons surface. The gas flows from the left to the right.

The k_v' values calculated from FLUENT results for 200 sccm and summarized in *Table 4* are of the same order of magnitude than the values obtained by numerical fit based on experimental data. A slowdown of the volatilization rate was calculated from the Upstream to the Downstream sample, in agreement with experimental observations. This demonstrates the validity of the simulation approach developed to represent the volatilization process.

However, two points can be discussed. At first, the CFD calculation suggested a higher difference between the volatilization rates at the Central and the Downstream samples surfaces

than those experimentally measured. This could be related to the fact that, in a first approach, it was assumed that the k_p' value was the same for the three samples. This was consistent, considering that the parabolic constant is known to only depend on the diffusion coefficient in the oxide scale and that similar results were obtained by XRD and SEM regarding the oxide scale analysis for the different samples. However, the hypothesis of a constant k_p' is thus questionable considering that the three samples were not oxidized in similar environments due to the $CrO_2(OH)_2$ volatilization. Indeed, variations of the k_p' in the presence of water vapor was highlighted in several studies [37,49]. Some parameters, which were not studied here, can have modified the oxide scale structure and thus the ions diffusion through it to explain this. At first, the oxide grain size, affecting the diffusion through the scale and therefore the k_p', could be slightly different between the samples. Young [51] discussed the fact that water vapor was shown to refine the grain structure of Cr_2O_3 scales grown on Ni25Cr. This was expected to be related to the adsorption of H_2O at oxide grain boundaries which would hinder the grain growth or to a modification of the oxide scale growth process induced by H_2O. This could be consistent with the fact that the sample oxidized in quasi-static laboratory air showed a little bit denser oxide than in wet flowing gas where the oxide had a more granular structure. Moreover, in their review, Saunders *et al.* [3] reported the presence of porosity in chromia scales formed in hot atmospheres containing water vapor, whereas in dry air the porosity was only observed at the alloy/oxide interface according to Henry *et al.* [52]. This phenomenon was attributed to a modification of transport mechanisms within the chromia scale. Water vapor could also favor the increase in cation vacancies and thus enhance chromium diffusion which was observed by Henry *et al.* [52], on pure Cr (99.7%) oxidized at 900 °C in flowing Ar-15%O_2 and Ar-15%H_2O, and by Arifin *et al.* [53] on Cr_2O_3 at 800 °C. They observed slightly porous particle arrangements in wet environment compared to dry one which could explain k_p' variations. This is consistent with the limitations of the current CFD model which does not consider any chemistry changes of the oxide scale.

Complementary experiments and CFD calculations were made by changing only the total gas flow to 500 sccm instead of 200 sccm to further analyze the validity of our simulation approach. As previously, k_v' values calculated thanks to FLUENT were compared to the experimental ones. The results are summarized in *Table 4*. At first, higher volatilization rates were measured for the three samples compared to tests performed with a gas flow rate of 200 sccm. This is consistent with the fact that for a similar oxidation duration, the faster $CrO_2(OH)_2$-enriched gas flow results in a higher Cr outflow from the sample surfaces. The results provided by simulation are another time very close to the experimental ones, which reinforces the validity of the simulation approach. The developed model thus offers a relevant tool to study the evolution of the gas phase composition and the Cr-loss due to the volatilization on a homogeneous Cr_2O_3 scale. It can be used to better design the laboratory experimental setups, when multiple samples are placed in the same furnace. Efforts are now necessary to get closer to most in-service conditions, considering higher flow rates and surface chemistry changes that can occur for longer exposure times. The fact that the experimental and simulation results obtained at two different gas flows were in a good agreement is promising for scaling-up. But increasing further the flow rate could lead to different samples behaviors. The model is thus validated only for low gas velocities. One challenging parameter would also remain the surface chemistry changes that are expected to occur for longer exposures in the wet flowing gas and for alloys containing higher Mn amounts. In particular, the formation of Mn and Cr-rich spinel on top of Cr_2O_3 will reduce the reactive surface and influence both the Cr_2O_3 growth and the volatilization rate.

Table 4 Comparison of the k_v' calculated based on numerical fit on experimental data and based on CFD calculations for tests performed at 200 and 500 sccm.

	k_v' – 200 sccm (mg.cm^{-2}.s^{-1})		k_v' – 500 sccm (mg.cm^{-2}.s^{-1})	
Position	**Experimental fit**	**FLUENT calculations**	**Experimental fit**	**FLUENT calculations**
Upstream	(4.5 ± 0.5) x 10^{-7}	4.2 x 10^{-7}	(5.5 ± 0.5) x 10^{-7}	6.7 x 10^{-7}
Central	(2.85 ± 0.1) x 10^{-7}	2.4 x 10^{-7}	(4.7 ± 0.1) x 10^{-7}	5.1 x 10^{-7}
Downstream	(2.6 ± 0.1) x 10^{-7}	1.45 x 10^{-7}	(3.9± 0.1) x 10^{-7}	4 x 10^{-7}

4. Conclusions

The volatilization of the Cr_2O_3 is of major concern for current industries for which alloys are expected to be exposed at high temperature in oxygen and water vapor rich environments. In this article, this phenomenon was investigated, coupling experimental tests and CFD calculation to represent the evolution of the gas composition during the tests. The aim was to enhance the understanding of the volatilization and the experimental practices which usually did not take into account the evolution of the gas composition during the experiments. The study focused on the first stages of the oxidation in a slow gas flow humid environment during which the chromia scale grows without any surface chemistry change.

Oxidations at 900 °C in laboratory air and in 74%N_2-18.5%O_2-7.5%H_2O flowing at 200 sccm during 500 h showed a strong influence of the position of the samples in a horizontal furnace on their oxidation behavior. This was suspected to be related to different volatilization rates at the samples surface due to an increase in the $CrO_2(OH)_2$ partial pressure in the gas mixture in the presence of water vapor. No influence of the water vapor on the oxide scale morphology was observed except for the formation of whiskers at the Upstream coupon surface.

A CFD model which has the advantage of being self-sufficient without the need of empirical relation to determine mass transfer coefficients, was developed. Calculations

confirmed the hypothesis made, showing modifications of the gas composition in presence of water vapor due to the volatilization reaction at the sample surface. As a consequence, it was demonstrated that the three samples were exposed to significantly different environments in the furnace as a function of their position along the flow direction. Indeed, the volatilization decreased onto the samples surface from the inlet up to the outlet of the furnace. A comparison of the simulated results with experimental tests carried out at a higher flow rate (500 sccm) confirmed the model validity and the previous hypotheses.

As a consequence, the fact that the mass loss can be limited by increasing the $CrO_2(OH)_2$ in the atmosphere or the gaseous diffusion layer (by decreasing the flow rate) suggests that the volatilization is limited by the mass transfer in the gas phase and not by the kinetics of the reaction.

Finally, this article showed striking evidences for the evolution of the gas composition during oxidation in the presence of water vapor and showed that it is essential to take it into account in order to provide correct interpretation of the results. The coupling of experiments with CFD simulations appears to be of major interest to deal with these issues and the developed model could allow future prediction of volatilization rates. The current CFD model allowed to describe the Cr-loss and gas phase changes during the initial oxidation stages of the 625-alloy in presence of water vapor at 900 °C. This brought promising results which appear as a starting point to consider in a future model surface chemistry changes and environmental parameters closer to most in-service conditions. The next challenge would consist in working with gas velocities between 3 and 7 $m.s^{-1}$ to be more representative of industrial practices and considering the formation of other oxides, especially Mn-rich spinel that can impact the volatilization rate. Studies are currently underway on these issues.

Aknowledgements

The authors thank the STAE Foundation (IRT Antoine de Saint-Exupéry, Toulouse) its financial support through 2020 Tremplins Actions. They thank Lounis Regad, Remi Garcia and Ronan

Mainguy for their help on the use of the oxidation rig. They also thank Yannick Thebault for his help on EDS analyses and Iréa Touche for her help on CFD calculations. Damien Connetable and Stephane Mathieu are gratefully acknowledged for fruitful discussions.

Data availability

The raw/processed data required to reproduce these findings cannot be shared at this time as the data also forms part of an ongoing study.

Bibliography

[1] G.R. Holcomb, Steam Oxidation and Chromia Evaporation in Ultra-Supercritical Steam Boilers and Turbines, ECS Trans. 16 (2009).

[2] M. Stanislowski, E. Wessel, K. Hilpert, T. Markus, L. Singheiser, Chromium Vaporization from High-Temperature Alloys : I . Chromia- Forming Steels and the Influence of Outer Oxide Layers Chromium Vaporization from High-Temperature Alloys I . Chromia-Forming Steels and the Influence of Outer Oxide Layers, J. Electrochem. Soc. 154 (2007) A295–A306. doi:10.1149/1.2434690.

[3] S.R.J. Saunders, M. Monteiro, F. Rizzo, The oxidation behaviour of metals and alloys at high temperatures in atmospheres containing water vapour: A review, 53 (2008) 775–837. doi:10.1016/j.pmatsci.2007.11.001.

[4] B. Pujilaksono, T. Jonsson, M. Halvarsson, I. Panas, J.E. Svensson, L.G. Johansson, Paralinear oxidation of chromium in O 2 + H 2O environment at 600-700 °c, Oxid. Met. 70 (2008) 163–188. doi:10.1007/s11085-008-9114-1.

[5] B.A. Pint, The effect of water vapor on Cr depletion in advanced recuperator alloys, Proc. GT2005. (2005) 1–8.

[6] G.R. Holcomb, Calculation of reactive-evaporation rates of chromia, Oxid. Met. 69 (2008) 163–180. doi:10.1007/s11085-008-9091-4.

[7] H. Buscail, R. Rolland, C. Issartel, F. Rabaste, F. Riffard, L. Aranda, M. Vilasi, Effects of water vapour on the oxidation of a nickel-base 625 alloy between 900 and 1100 ° C, J. Mater. Sci. (2011) 5903–5915. doi:10.1007/s10853-011-5544-2.

[8] P.J. Meschter, E.J. Opila, N.S. Jacobson, Water vapor-mediated volatilization of high-temperature materials, Annu. Rev. Mater. Res. 43 (2013) 559–588. doi:10.1146/annurev-matsci-071312-121636.

[9] B. Henri, R. Raphaël, I. Christophe, R. Frédéric, R. Françoise, P. Sébastien, Influence of water vapour on a Nickel-Based alloy oxidation ., Defect Diffus. Forum. 323–325 (2012) 309–314. doi:10.4028/www.scientific.net/DDF.323-325.309.

[10] D. Caplan, M. Cohen, The Volatilization of Chromium Oxide, J. Electrochem. Soc. 108 (1961) 438. doi:10.1149/1.2428106.

[11] R.T. Grimley, R.P. Burns, M.G. Inghram, Thermodynamics of the vaporization of Cr2O3: Dissociation energies of CrO, CrO2, and CrO3, J. Chem. Phys. 34 (1961) 664–667. doi:10.1063/1.1701005.

[12] H.C. Graham, H.H. Davis, Oxidation / Vaporization Kinetics of Cr2O3, J. Am. Ceram. Soc. 54 (1973) 89–93.

[13] Y.W. Kim, G.R. Belton, The thermodynamics of Volatilization of Chromic Oxide: Part I. The species CrO3 and CrO2OH, Metall. Trans. 5 (1974) 1811–1816. doi:10.1007/BF02644145.

[14] N.S. Jacobson, M.A. Kuczmarski, B.A. Kowalski, Vaporization of Protective Oxide Films into Different Gas Atmospheres, Springer US, 2020. doi:10.1007/s11085-019-09921-1.

[15] G.C. Fryburg, R.A. Miller, F.J. Kohl, C.A. Stearns, Volatile Products in the Corrosion of Cr, Mo, Ti, and Four Superalloys Exposed to O 2 Containing H 2 O and Gaseous NaCl,

J. Electrochem. Soc. 124 (1977) 1738–1743. doi:10.1149/1.2133147.

[16] E.J. Opila, D.L. Myers, N.S. Jacobson, I.M.B. Nielsen, D.F. Johnson, J.K. Olminsky, M.D. Allendorf, Theoretical and Experimental Investigation of the Thermochemistry of CrO2(OH)2, J. Phys. Chem. 111 (2007) 1971–1980. doi:10.1021/jp0647380.

[17] M. Romedenne, R. Pillai, S. Dryepondt, B.A. Pint, Effect of Water Vapor on Lifetime of 625 and 120 Foils During Oxidation Between 650 and 800 °C, Oxid. Met. (2021). doi:10.1007/s11085-021-10069-0.

[18] T. Sand, C. Geers, Y. Cao, J.E. Svensson, L.G. Johansson, Effective Reduction of Chromium-oxy-hydroxide Evaporation from Ni-Base Alloy 690, Oxid. Met. 92 (2019) 259–279. doi:10.1007/s11085-019-09935-9.

[19] M. Schütze, D. Renusch, M. Schorr, Chemical-mechanical failure of oxide scales on 9% Cr steels in air with H2O, Mater. High Temp. 22 (2005) 113–120. doi:10.1179/mht.2005.013.

[20] X. Peng, J. Yan, Y. Zhou, F. Wang, Effect of grain refinement on the resistance of 304 stainless steel to breakaway oxidation in wet air, Acta Mater. 53 (2005) 5079–5088. doi:10.1016/j.actamat.2005.07.019.

[21] H. Asteman, J. Svensson, L. Johansson, Evidence for Chromium Evaporation Influencing the Oxidation of 304L : The Effect of Temperature and Flow Rate, Oxid. Met. 57 (2002) 193–216.

[22] H. Asteman, Oxidation of 310 steel in H2O / O2 mixtures at 600 °C: the effect of water-vapour-enhanced chromium evaporation, Corros. Sci. 44 (2002) 2635–2649.

[23] H. Asteman, J. Svensson, M. Norell, L. Johansson, Influence of Water Vapor and Flow Rate on the High-Temperature Oxidation of 304L; Effect of Chromium Oxide Hydroxide Evaporation, Oxid. Met. 54 (2000) 11–26.

[24] V.P. Deodeshmukh, Long-term performance of high-temperature foil alloys in water vapor containing environment. Part I: Oxidation behavior, Oxid. Met. 79 (2013) 567–578. doi:10.1007/s11085-012-9343-1.

[25] P. Huczkowski, W. Lehnert, H. Angermann, A. Chyrkin, E. Hejrani, W.J. Quadakkers, R. Pillai, D. Gr, Effect of gas flow rate on oxidation behaviour of alloy 625 in wet air in the temperature range 900 – 1000 °C, Mater. Corros. 68 (2017) 159–170. doi:10.1002/maco.201608831.

[26] J. Xiao, N. Prud'Homme, N. Li, V. Ji, Influence of humidity on high temperature oxidation of Inconel 600 alloy: Oxide layers and residual stress study, Appl. Surf. Sci. 284 (2013) 446–452. doi:10.1016/j.apsusc.2013.07.117.

[27] Z. Liang, T. Guo, S. Deng, Q. Zhao, High-temperature corrosion of an Fe–Ni-based alloy HR6W under various conditions at 750 °C and 810 °C: Effect of the temperature, water vapor, simulated ash and SO2, Mater. Chem. Phys. 256 (2020) 123670. doi:10.1016/j.matchemphys.2020.123670.

[28] R.A. Golden, E.J. Opila, A method for assessing the volatility of oxides in high-temperature high-velocity water vapor, J. Eur. Ceram. Soc. 36 (2016) 1135–1147. doi:10.1016/j.jeurceramsoc.2015.11.016.

[29] S. Chandra-Ambhorn, P. Wongpromrat, T. Thublaor, W. Chandra-Ambhorn, Effect of water vapour on the high temperature oxidation of stainless steels, Solid State Phenom. 300 (2020) 107–134. doi:10.4028/www.scientific.net/SSP.300.107.

[30] M. Mermoux, C. Duriez, O. Coindreau, High temperature Zircaloy-4 oxidation in water vapour-containing environments examined with Raman imaging and labelled oxygen, Corros. Sci. 184 (2021) 109351. doi:10.1016/j.corsci.2021.109351.

[31] D. Zhu, X. Wang, J. Zhao, J. Lu, Y. Zhou, C. Cai, J. Huang, G. Zhou, Effect of water

vapor on high-temperature oxidation of NiAl alloy, Corros. Sci. 177 (2020) 108963. doi:10.1016/j.corsci.2020.108963.

[32] D.J. Young, B.A. Pint, Chromium Volatilization Rates from Cr2O3 Scales into Flowing Gases Containing Water Vapor, Oxid. Met. 66 (2006) 137–152. doi:10.1007/s11085-006-9030-1.

[33] A. Chyrkin, C. Bo, J. Barnikel, F. Schmitz, W.J. Quadakkers, Oxidation behaviour and microstructural stability of alloy 625 during long-term exposure in steam, (2014) 6127–6142. doi:10.1007/s10853-014-8344-7.

[34] M.D. Bender, R.C. Klug, presented at ASME Turbo Expo 2014: Turbine Technical Conference and Exposition, in: Dusseldorf, Germany, 2014: p. V01BT24A007-1–V01BT24A007-10.

[35] A. Al-Masri, M. Peksen, L. Blum, D. Stolten, A 3D CFD model for predicting the temperature distribution in a full scale APU SOFC short stack under transient operating conditions, Appl. Energy. 135 (2014) 539–547. doi:10.1016/j.apenergy.2014.08.052.

[36] G.R. Holcomb, D.E. Alman, The effect of manganese additions on the reactive evaporation of chromium in Ni – Cr alloys, Scr. Mater. 54 (2006) 1821–1825. doi:10.1016/j.scriptamat.2006.01.026.

[37] P. Berthod, L. Aranda, Influence of Water Vapour on the Rate of Oxidation of a Ni–25wt.%Cr Alloy at High Temperature, Oxid. Met. 79 (2013) 517–527. doi:10.1007/s11085-012-9339-x.

[38] M. Hänsel, W.J. Quadakkers, D.J. Young, Role of Water Vapor in Chromia-Scale Growth at Low Oxygen Partial Pressure, Oxid. Met. 59 (2003) 285–301.

[39] T.D. Nguyen, J. Zhang, D.J. Young, Growth of Cr2O3 blades during alloy scaling in wet CO2 gas, Corros. Sci. 133 (2018) 432–442. doi:10.1016/j.corsci.2018.01.045.

[40] B. Pieraggi, C. Rolland, P. Bruckel, Morphological characteristics of oxide scales grown on H11 steel oxidised in dry or wet air, Mater. High Temp. 22 (2005) 61–68. doi:10.1179/mht.2005.007.

[41] X.G. Zheng, D.J. Young, High-temperature corrosion of Cr2O3-forming alloys in CO-CO2-N2 atmospheres, Oxid. Met. 42 (1994) 163–190. doi:10.1007/BF01052021.

[42] G.M. Raynaud, R.A. Rapp, in-Situ Observation of Whiskers, Pyramids and Pits During the High Temperature Oxidation of Metals, Oxid. Met. 21 (1984) 89–102.

[43] P. Berthod, F. Allègre, E. Kretz, Influence of Titanium on the High Temperature Oxidation and Chromia Volatilization of Ternary Ni–Cr–C Alloys, Oxid. Met. 86 (2016) 581–595. doi:10.1007/s11085-016-9656-6.

[44] H. Nagai, M. Okabayashi, Deleterious effect of Ti addition on the oxidation resistance of Ni-20Cr alloy, Trans. Japan Inst. Met. 22 (1981) 691–698.

[45] S. Cruchley, H.E. Evans, M.P. Taylor, M.C. Hardy, S. Stekovic, Chromia layer growth on a Ni-based superalloy: Sub-parabolic kinetics and the role of titanium, Corros. Sci. 75 (2013) 58–66. doi:10.1016/j.corsci.2013.05.016.

[46] K.A. Al-Hatab, M.A. Al-Bukhaiti, U. Krupp, Cyclic oxidation kinetics and oxide scale morphologies developed on alloy 617, Appl. Surf. Sci. 318 (2014) 275–279. doi:10.1016/j.apsusc.2014.04.199.

[47] R.E. Lobnig, H.P. Schmidt, K. Hennesen, H.J. Grabke, Diffusion of cations in chromia layers grown on iron-base alloys, Oxid. Met. 37 (1992) 81–93. doi:10.1007/BF00665632.

[48] N. Ramenatte, A. Vernouillet, S. Mathieu, A. Vande Put, M. Vilasi, D. Monceau, A comparison of the high-temperature oxidation behaviour of conventional wrought and laser beam melted Inconel 625, Corros. Sci. 164 (2020).

doi:10.1016/j.corsci.2019.108347.

[49] L. Aranda, T. Schweitzer, L. Mouton, S. Mathieu, O. Rouer, P. Villeger, E. Conrath, T. Schweitzer, L. Mouton, S. Mathieu, O. Rouer, P. Villeger, L. Aranda, T. Schweitzer, L. Mouton, S. Mathieu, O. Rouer, P. Villeger, Materials at High Temperatures Kinetic and metallographic study of oxidation at high temperature of cast Ni 25Cr alloy in water vapour rich air Kinetic and metallographic study of oxidation at high temperature of cast Ni 25Cr alloy in water vapour rich ai, Mater. High Temp. 32 (2015) 530–538. doi:10.1179/1878641314Y.0000000041.

[50] J. Froitzheim, J. Electrochem, B. Soc, J. Froitzheim, H. Ravash, E. Larsson, L.G. Johansson, J.E. Svensson, Investigation of Chromium Volatilization from FeCr Interconnects by a Denuder Technique, J. Electrochem. Soc. 157 (2010) B1295–B1300. doi:10.1149/1.3462987.

[51] D.J. Young, Effects of water vapour on the oxidation of chromia formers, Mater. Sci. Forum. 595-598 PA (2008) 1189–1197. doi:10.4028/www.scientific.net/msf.595-598.1189.

[52] S. Henry, J. Mougin, Y. Wouters, J.P. Petit, A. Galerie, Characterization of chromia scales grown on pure chromium in different oxidizing atmospheres, Mater. High Temp. 17 (2000) 231–234. doi:10.1179/mht.2000.17.2.008.

[53] S.K. Arifin, M. Hamid, A.N. Berahim, M.H. Ani, Effects of water vapor on protectiveness of Cr2O3 scale at 1073 K, IOP Conf. Ser. Mater. Sci. Eng. 290 (2018). doi:10.1088/1757-899X/290/1/012085.

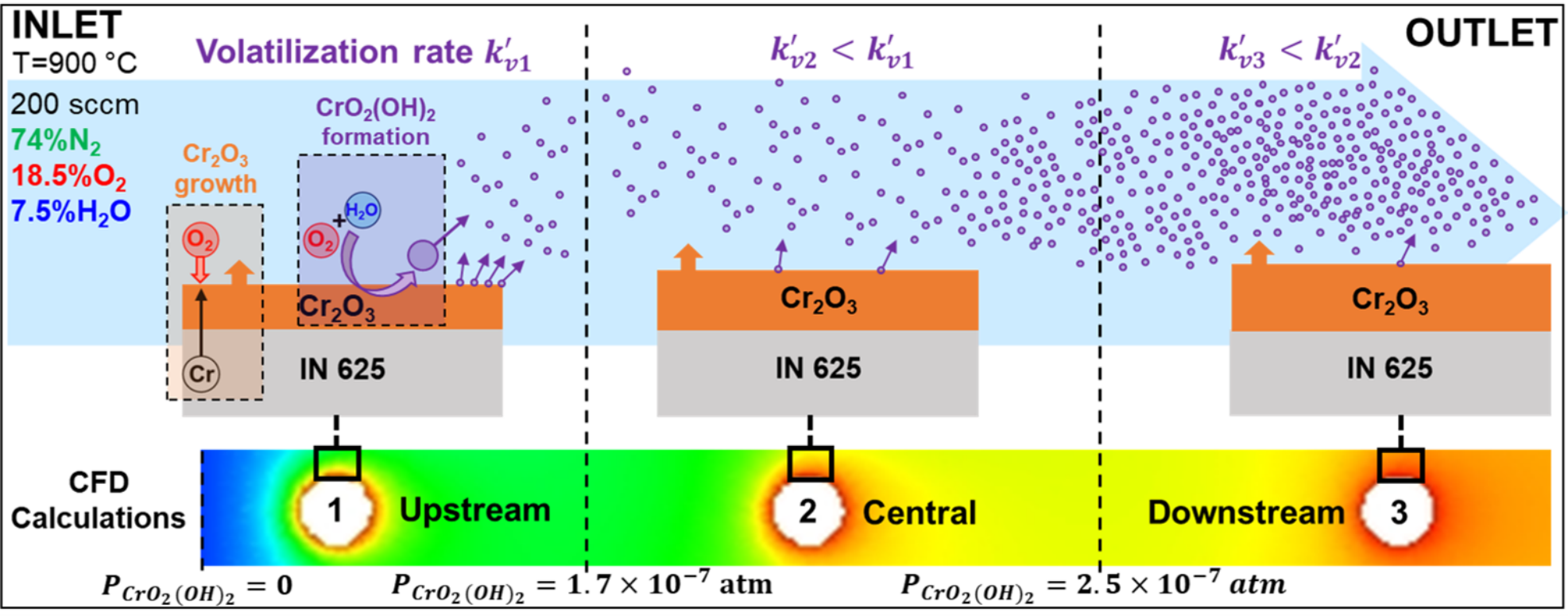
INLET
T=900 °C
200 sccm
74%N2
18.5%O2
7.5%H2O
Volatilization rate k'_{v1}
$k'_{v2} < k'_{v1}$
$k'_{v3} < k'_{v2}$
OUTLET
$CrO_2(OH)_2$ formation
Cr_2O_3 growth
H_2O
O_2
O_2
Cr
Cr_2O_3
IN 625
Cr_2O_3
IN 625
Cr_2O_3
IN 625
CFD Calculations
1
Upstream
2
Central
Downstream
3
$P_{CrO_2(OH)_2} = 0$
$P_{CrO_2(OH)_2} = 1.7 \times 10^{-7}$ atm
$P_{CrO_2(OH)_2} = 2.5 \times 10^{-7}$ atm